

AN ANALYSIS OF THE PRECISION OF A DEM OBTAINED FROM SPOT DATA

Auke de Haan, Ph.D. student

Politecnico di Milano
Dipartimento I.I.A.R. - Sezione di Rilevamento
Piazza Leonardo da Vinci 32
20133 Milano
ITALY

Commission IV

ABSTRACT:

The suitability of stereo SPOT imagery for the production of DEM's for large areas with modest precision has been demonstrated by many research centres. Here the different aspects determining the precision of such a DEM are considered. Important factors are the quality of the reconstruction of the imaging geometry, the precision of the measurement of conjugate image points, the intersection geometry of the imaging rays, and the fitting of a continuous surface to the determined set of points. The determination of the imaging geometry is dealt with in detail.

KEYWORDS: SPOT, DEM, aerotriangulation, accuracy, image matching.

1. INTRODUCTION

In 1992 SPOT entered the seventh year of operation of continuous worldwide imaging. In the past six years, many of the research centres of the ISPRS community developed methods for geometric evaluation of SPOT data and carried out experiments to verify the suitability of the imagery for topographic mapping (Dowman, 1992), (Heipke and Kornus, 1991), (Konecny, 1988), (Priebbenow, 1988), (Chen et al., 1988). Most reported precisions in the 10 m level. At the moment aerotriangulation and DEM production with SPOT data are shifting from research to routine practise.

The production of a DEM from stereo SPOT data consists of a three step procedure:

aerotriangulation, in which the imaging geometry is determined from image measurements, auxiliary data and ground control;

the measurement of a set of conjugate image points, and determination of their 3-D ground position by intersection of imaging rays;

the fitting of a (piecewise) smooth surface to the obtained (irregularly distributed) points, in order to have a continuous representation of the terrain.

In the following, the contribution of each of these steps to the final precision of the derived DEM is reviewed. The modelling of the imaging geometry is considered in detail.

2. AEROTRIANGULATION

In bundle block adjustments with aerial photographs, object coordinates are determined from image measurements in a very precise and efficient way (Grün, 1982). In these, the measurement of the image coordinates $(x_{p,j}, y_{p,j})$ of a point p of image j leads to the introduction of two collinearity equations,

$$x_{p,j} = -f \frac{r_{11}(X_p - X_{o,j}) + r_{12}(Y_p - Y_{o,j}) + r_{13}(Z_p - Z_{o,j})}{r_{31}(X_p - X_{o,j}) + r_{32}(Y_p - Y_{o,j}) + r_{33}(Z_p - Z_{o,j})}$$

$$y_{p,j} = -f \frac{r_{21}(X_p - X_{o,j}) + r_{22}(Y_p - Y_{o,j}) + r_{23}(Z_p - Z_{o,j})}{r_{31}(X_p - X_{o,j}) + r_{32}(Y_p - Y_{o,j}) + r_{33}(Z_p - Z_{o,j})}$$

The collinearity equations directly relate the observed image coordinates to the unknown object coordinates (X_p, Y_p, Z_p) and the parameters describing the projection geometry of image j ($r_{11}..r_{33}$ and $X_{o,j}..Z_{o,j}$).

The high precision of the procedure originates from the fact that the collinearity equations provide a direct link between the image coordinates to the object coordinates. Thus relative orientation and model coordinates are bypassed and self calibration parameters can be included in the adjustment to correct systematic errors. Block adjustments are efficient because the simultaneous treatment of a (large) number of images greatly reduces the number of necessary ground control points.

This high precision and efficiency is also obtained in bundle block adjustments with SPOT data. There are, however, significant differences with respect to adjustments with data from aerial images. These include the different nature of the imagery, different perspective relations and a different geometry for the intersecting imaging rays.

The five most important particularities of bundle block adjustments with SPOT data are:

- each row is central projection (instead of each image);
- the aperture angle is very small (4°) (instead of 60° - 120°);
- successive images of pass are successive parts of a continuous strip (they are not independent and not overlapping);
- the imagery is digital (instead of film based);
- auxiliary data on image geometry is available.

Figures 1-4 illustrate the first three differences.

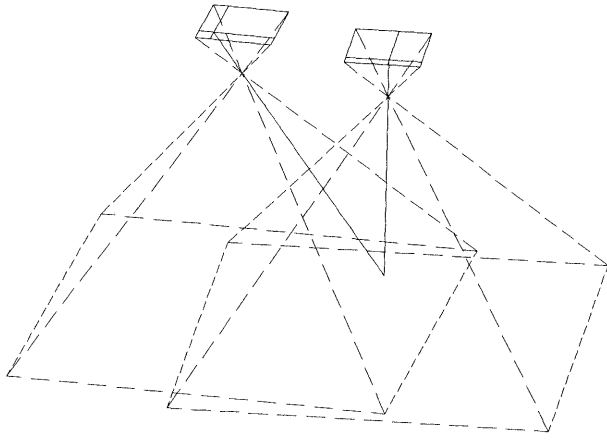


Fig. 1 - Intersection geometry of two imaging rays from a stereopair of aerial photographs.

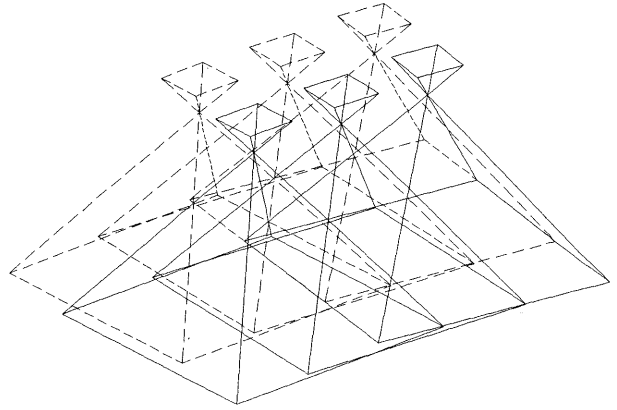


Fig. 3 - Block of aerial photographs.

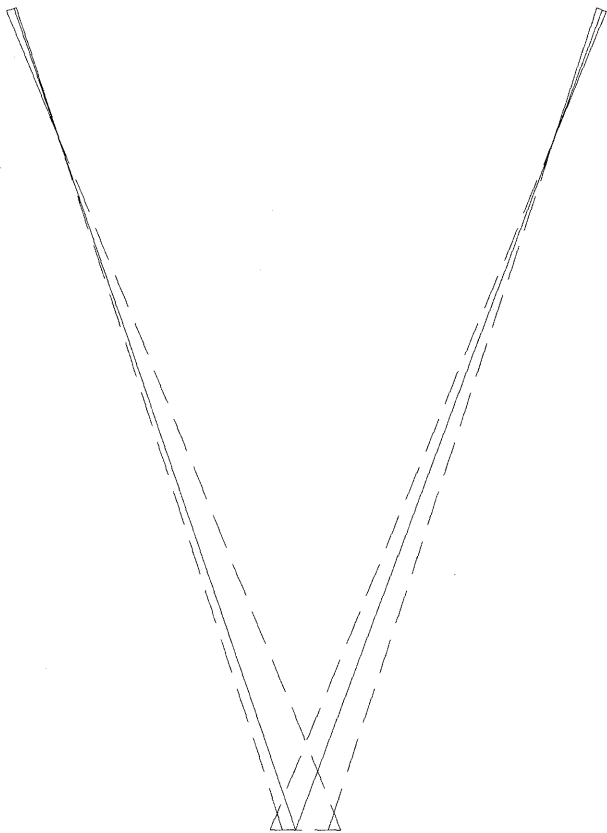


Fig. 2 - Intersection geometry of two imaging rays from a stereopair of SPOT images (off-nadir angles: 20° East / 20° West).

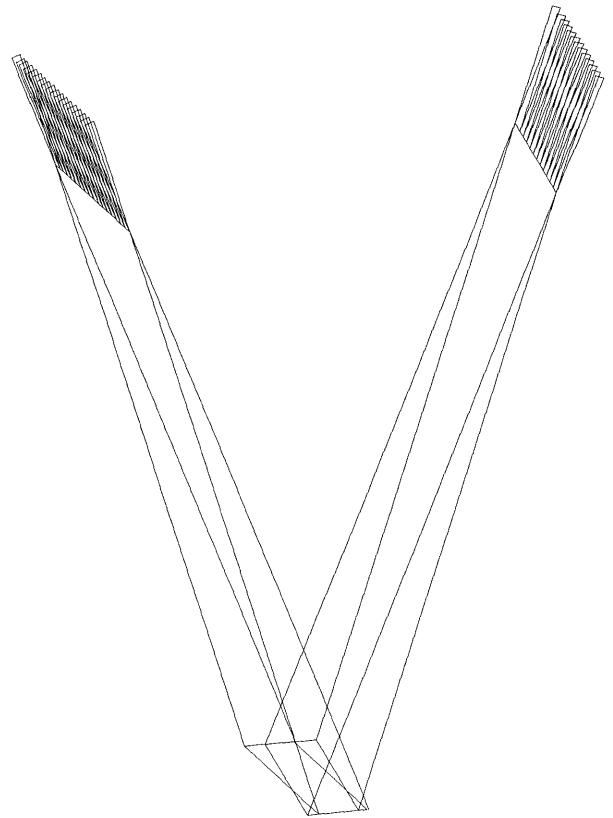


Fig. 4 - Block of two strips of successive SPOT images (off-nadir angles: 20° East / 20° West).

In order to formulate the collinearity equations for SPOT data, image coordinates (*row, column*) of a point *p* in strip *j* are transformed to the instrumental coordinates ($x_{p,j}, y_{p,j}$) corresponding to the time of imaging *t*,

$$t = t_{row_3000} + 1.504ms*(row-3000),$$

$$x_{p,j} = (3000.5-column)*13micron$$

$$y_{p,j} = 0$$

While the *y*-coordinate (perpendicular to the detector array) is zero by definition, *x* equals the column distance to the image centre scaled with the detector spacing.

The collinearity equations are now formulated in the following way:

$$x_{p,j} = -f \frac{r_{11}(X_p - X_s(t)) + r_{12}(Y_p - Y_s(t)) + r_{13}(Z_p - Z_s(t))}{r_{31}(X_p - X_s(t)) + r_{32}(Y_p - Y_s(t)) + r_{33}(Z_p - Z_s(t))}$$

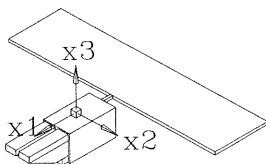
$$0 = -f \frac{r_{21}(X_p - X_s(t)) + r_{22}(Y_p - Y_s(t)) + r_{23}(Z_p - Z_s(t))}{r_{31}(X_p - X_s(t)) + r_{32}(Y_p - Y_s(t)) + r_{33}(Z_p - Z_s(t))}$$

Due to the dynamic imaging, all parameters describing the projection geometry are functions of time. The projection centre equals the current satellite's position. The elements of the rotation matrix ($r_{11}...r_{33}$) depend both on the satellite's position - and velocity vector and on the changing platform attitude.

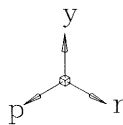
Whereas with aerial photogrammetry there is little to choose in the formulation of the mathematical model, with SPOT imagery many valid alternatives exist, especially for the modelling of the satellite's orbit and for the attitude of its platform.

2.1 Orbit

The orbital arc, which was completed by the satellite during image acquisition has to be reconstructed for two purposes: firstly, because it provides the projection centre of each image row, and secondly because it defines the target attitude of the satellite's platform (fig. 5).



actual platform attitude



target attitude

$$p = \frac{1}{\|\dot{X}(t) \times X(t)\|} \dot{X}(t) \times X(t)$$

$$r = y \times p$$

$$y = \frac{1}{\|X(t)\|} X(t)$$

Fig. 5 - Definition of the target attitude with the satellite's (geocentric) position vector X and its (inertial) velocity vector \dot{X} .

The target attitude corresponds to a perfect alignment of the satellite fixed triad $\{x1, x2, x3\}$ with the triad $\{p, r, y\}$ (pitch, roll, yaw axes), which is defined with the satellite's position and velocity vector.

The satellite's trajectory, from the time of imaging of the first to that of the last image line, is completely determined by the external forces, which accelerate the satellite. Due to the high speed of image acquisition (1 image is completed in 9 seconds), the time interval, for which the orbit has to be reconstructed, is always short, even if several successive images are treated. Besides, the accuracy needed is quite modest, compared to the centimetre precision requirements, with which satellite geodesists are used to work (Sansò and Rummel, 1988).

The contribution of non gravitational forces to the satellite's acceleration is smaller than $1 \cdot 10^{-5} m/s^2$ and can therefore be neglected. Starting with an initial position - and velocity vector ($X(t_0)...Z(t_0)$), the orbital arc can be reproduced with the following equations of motion,

$$\frac{d}{dt} \begin{pmatrix} X(t) \\ Y(t) \\ Z(t) \\ \dot{X}(t) \\ \dot{Y}(t) \\ \dot{Z}(t) \end{pmatrix} = \begin{pmatrix} \dot{X}(t) \\ \dot{Y}(t) \\ \dot{Z}(t) \\ dU/dX \\ dU/dY \\ dU/dZ \end{pmatrix}$$

with *U* the gravitational potential of the earth. The satellite's acceleration vector, the gradient vector of *U*, can be divided in three different parts. The largest part (about $7.4 m/s^2$) is geocentric: it corresponds to a homogeneous, spherical earth. This term alone would lead to an ellips-shaped Keplerian orbit, with the orbital plane fixed in inertial space. The part second in magnitude is the so called J_2 term (about $8 \cdot 10^{-3} m/s^2$), which correspond to the gravitational effect of the earth's flattening. SPOT's orbit is chosen in such a way that the J_2 term provides the drift of the orbital plane necessary to remain sunsynchronous. The remaining part of gravitational acceleration, due to the effect of irregularities in the mass distribution of the earth, is the smallest in magnitude (about $1 \cdot 10^{-4} m/s^2$).

The positioning error caused by neglecting an acceleration a_e for an orbital arc of *T* seconds equals $a_e T^2$. When accepting a model-(in)accuracy of 1m for orbit reconstructing, the central term alone is sufficient for arcs up to 11 s (1.2 image), while a force model including also the J_2 term is adequate for arcs of up to 11 images.

Two alternatives exist for a rigorous modelling of the orbital arc. The first is numerically integrating the equations of motion. The second, more elegant, method is taking the analytic solution for the Keplerian orbit, and add first order perturbations to these parameters caused by the J_2 term.

Auxiliary data includes sufficiently precise velocity data and less accurate position data. The orbit reconstruction, which was reduced to a 6 parameter problem by the introduction of the knowledge of the force field, is further limited to a three parameter problem by the auxiliary data. These remaining three parameters have to be determined predominantly by ground control in the bundle adjustment.

2.2 Platform attitude

The satellite's attitude control system constantly tries to align the platform to the target attitude defined in fig. 5 by applying torques. It continuously receives information on the current platform attitude from gyro's, which provide the rate of change about the pitch, roll and yaw axes.

These rates are available to the user as auxiliary data at intervals of 0.125 s. Integration of these values provides the variations in the angles during the period of image acquisition. Figures 6-8 show typical patterns for the ground effects of these variations, as they result from (integration of) the error attitude velocity data (based on an off-nadir angle of 20°).

The effect depends on the satellite altitude H and the off-nadir viewing angle θ , and can be computed in the following way. In the $\{p,r,y\}$ frame, the coordinates of vector pointing from the imaged ground point to the position of the satellite, is approximately equal to $(H \tan(\theta), 0, H)^t$. The effect on the imaging ray at ground level of a rotation of the platform about the pitch, roll and yaw axes is equal to the product of the angle (in radians) and the length of the imaging ray in the r-y -, p-y - and p-r plane respectively.

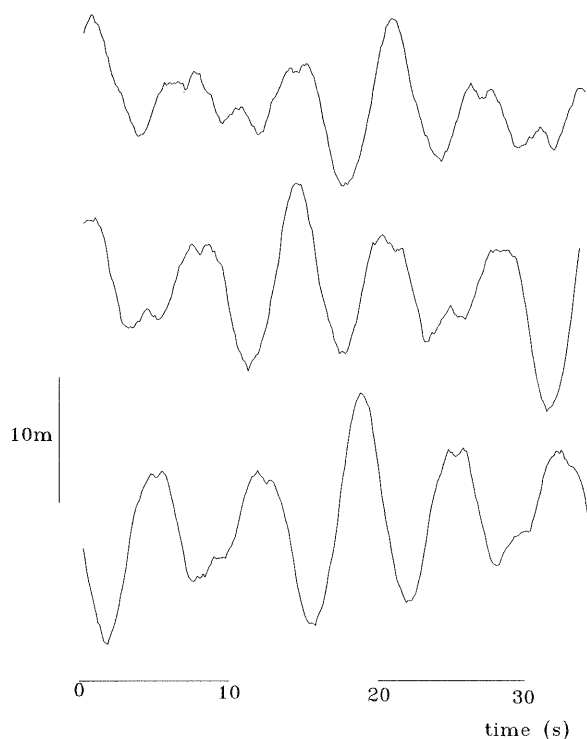


Fig. 6 - Typical patterns for the ground effect on the imaging ray of variations in pitch a the time interval of four successive images (off-nadir angle: 20°).

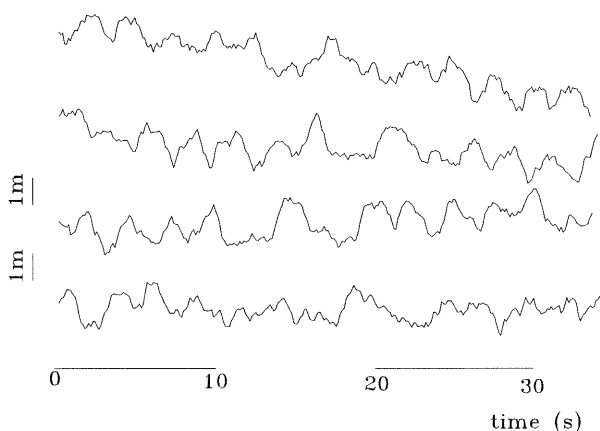


Fig. 7 - Typical patterns for the ground effect on the imaging ray of variations in roll for a time interval of four successive images (off-nadir angle: 20°).

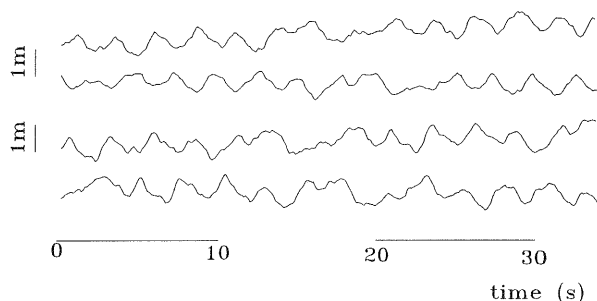


Fig. 8 - Typical patterns for the ground effect on the imaging ray of variations in yaw for a time interval of four successive images (off-nadir angle: 20°).

The figures show that the satellite is able to keep the platform attitude very stable: maximum ground effects of variations in pitch, roll and yaw are limited to about 10 m, 3 m and 1 m respectively. The use of the error angle rates leads to the corresponding maximum improvements in positioning precision. Most approaches integrate the velocities beforehand and then introduce the results as error-free in the bundle adjustment. Alternatively, the data can be introduced as additional observations, in observation equations equalling them to the derivative of the unknown pitch, roll and yaw functions. Thus, these functions can be estimated simultaneously from all data (velocity data, image measurements and ground control). Note that the approximating functions, which are fitted to the velocity data, have to be quite flexible to follow the variation patterns. This does not present a problem, because the large number of available velocities allow for a functions with many parameter (e.g. cubic splines).

The satellite is able to determine the target platform orientation only with a certain precision. The orientation, to which it tries to align the platform, i.e. the mean values around which the patterns of fig.s 6-8 oscillate, is not exactly identical to the right (nominal) target attitude. Besides, the difference between the two orientations slowly changes with time due to gyrodraft. Therefore, besides the high frequency variations, which are described by the velocity data, a slow trend remains, which has to be determined by image measurements and ground control. Low order polynomials can be introduced to model this trend. Experiments of Priebbenow showed that low order polynomials lead to better results than constants. With strips of four successive images the best results were obtained with first degree polynomials for (the remaining) roll and yaw and a second degree polynomial for (the remaining) pitch (Priebbenow, 1992).

2.3 The optical instrument

After orbit and attitude, the characteristics of the optical instrument are the third and last aspect of the imaging process, which has to be modelled. This can be carried out with the end detector look angles a, b, c and d , which are provided as auxiliary data. (In SPOT terminology, these are called ψ_x of first detector, ψ_x of last detector, ψ_y of first detector and ψ_y of last detector respectively). These describe the exact orientation of the scanline with respect to the $\{x_1, x_2, x_3\}$ frame. The angles a and b , which are about 0.5° in magnitude, account for a small offset of the detector arrays in the focal plane. The angles c and d incorporate the degree of the off-nadir viewing established by the strip selection mirror and can vary between -29° and $+27^{\circ}$ and -27° and $+29^{\circ}$ respectively. They also provide a precise value for the focal length (de Haan, 1991). The four look angles are constant for each strip of successive images. Mostly, they are considered error free. However, especially for c and d , which are affected by the uncertainty about the exact position of the strip selection mirror, it may be worthwhile to introduce them as

parameters in the adjustment, so that their estimated values can be improved with the other observational data.

2.4 Conclusions

In the aerotriangulation, three groups of image geometry parameters, describing respectively orbit, attitude and optical instrument, and the ground coordinates of the measured image points are determined simultaneously with the following types of data:

- auxiliary data (satellite ephemeris, pitch -, roll - and yaw velocities and end detector look angles);

- measured image coordinates;

- ground control points.

By careful modelling and the use of auxiliary data the imaging geometry can be determined with sufficient precision with a limited number of ground control:

- apart from an orbital shift, the ephemeris data and orbital mechanics alone are sufficient for an accurate reconstruction of the orbital arc;

- apart from an unknown constant or slow trend, the attitude angle velocities allow for a full description of variations of pitch, roll and yaw during the image acquisition period;

- the end detector look angles provide a complete description of the central projection geometry of the optical instrument;

- by pass processing, the effort needed to determine the geometry of a strip of successive images is equal to that of a single image.

The importance of reduction of ground control is illustrated by the fact that Murray and Newby estimated the cost of ground control to be about one third of total cost of mapping with SPOT data (Murray and Newby, 1990).

The concept of accurate modelling and pass processing was successfully applied with (mono) Landsat data by Friedmann et al. as early as 1983 (Friedmann et al., 1983). Its suitability for (stereo) SPOT data was demonstrated by the OEEPE test on triangulation with SPOT data (Dowman, 1992).

3 THE INTERSECTION GEOMETRY AND THE PRECISION OF CONJUGATE POINTS

Assume the imaging geometry has been determined with sufficient precision in a triangulation adjustment. The ground position of a point measured in two images can then be found by determining the point of intersection of the corresponding imaging rays (fig. 2). The next steps in the analysis are therefore the precision of image measurement and the intersection geometry of imaging rays.

3.1 The geometry of intersecting imaging rays

Due to the orbital characteristics of SPOT, the scanlines of different passes are almost parallel. The plane defined by the intersecting imaging rays is therefore practically aligned with the detector arrays and near perpendicular to both orbital planes.

This causes a remarkable separation between the positioning contributions of the row and column measurements: while the two row measurements determine the ground point's along track position with one degree of redundancy, the two column measurements

provide just enough information to determine its across track position and height.

From intersection geometry alone (i.e. assuming perfect knowledge of imaging geometry and row and column measurements of equal precision), the along track position is determined with the best precision thanks to the redundancy. Of the other two coordinates, across track position is better determined than height, because the angle of intersection is always sharp. Fig. 9 shows positioning accuracies for the intersection geometries of stereo pairs with different off-nadir viewing angles, assuming image measurement rmse's of 0.25 and 0.5 pixel.

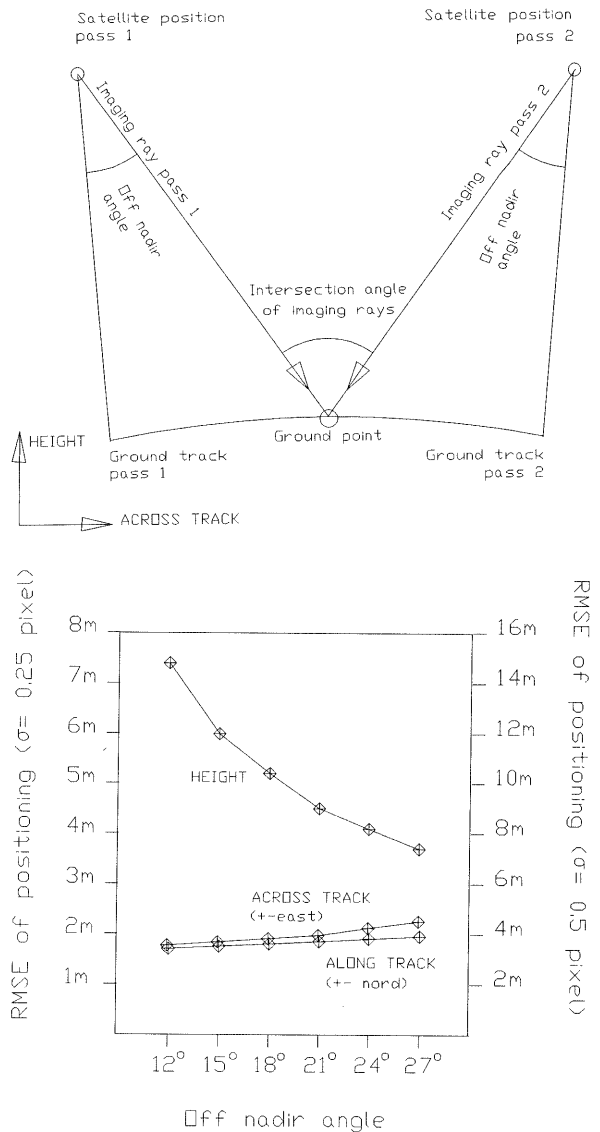


Fig. 9 - The intersection geometry of the imaging rays and the resulting positioning precision (assuming perfect knowledge of imaging geometry).

The fact that the measurement of conjugate image points provides redundancy only in the along track direction has also consequences for the determinability of the pitch, roll and yaw functions. While the pitch function can be determined from all conjugate image point measurement, the roll and yaw functions have to be determined exclusively from ground control.

Empirical results seem to indicate however, that intersection geometry is not a decisive factor in determining the rank of the positioning precisions in the

three coordinate directions: in the OEEPE test on triangulation with SPOT data, it was concluded that height is better determined than planimetry (Dowman, 1992). Maybe, image geometry errors affect planimetry more than height.

3.2 The precision of the measurement of conjugate image points.

Conjugate image points can be measured in many ways. Mostly transparencies are used in analytical plotters. These transparencies are derived with filmprinters from the original digital data. A more logical alternative is to use the original data in digital photogrammetric systems. These however usually do not offer stereo vision. Digital photogrammetric systems are also more suited for (partially) automated tasks, in which the image data must be available in its digital form.

No matter how points are measured, manually or automatically, in transparencies or in soft copies, the decisive factor for the precision of point identification is the distribution and magnitude of grey level gradients in the neighbourhood of the point. The larger and the better distributed the grey level gradients around a point, the preciser it can be located in the imagery. It is therefore advantageous to apply an interest operator for the selection of candidate ground control points and DEM points.

In the test of working group III/4 of the ISPRS on image matching, least squares matching and other precise algorithms obtained r.m.s.e.'s of 0.1 to 1.5 pixels for images of different complexity (Gülch, 1988). Although the test was carried out with scanned transparencies and with relatively large scale imagery (1:20 - 1:30000), the same range seems to be indicative for stereo SPOT images.

Experiments have been carried out in Milan to estimate the precision of (manual) conjugate image point measurements. Two different methods were used, repeated measurement of the same image points and weight estimation with the residuals of triangulation adjustments. The latter method (Kubik, 1970) consists of repeated adjustments, in each of which weights are estimated for groups of measurements. These are then introduced to a successive adjustment. This is repeated until the weight estimates converge to a constant value.

Both methods led to the same results. When points are chosen with much care, they can be measured with a r.m.s.e. of 0.25 pixels. Results of Westin (Westin, 1990) confirm this figure. Measurements of average points have a r.m.s.e. of 0.5 pixel, both for row and column coordinate. The points, which offer the highest measurement precision are excellent ground control points. Their distribution is usually not dense enough for the derivation of a high resolution DEM. Conjugate image points, which can be determined with a r.m.s.e. of 0.5 pixel can easily be found by thousands and are therefore more suited for this purpose.

4 HEIGHT INTERPOLATION EFFECTS

The last step in DEM production is the fitting of a (piecewise) smooth surface to the obtained irregularly distributed points. The continuous representation of the terrain is then the final product.

Many different interpolation strategies have been proposed, which are beyond the scope of this paper, and will not be discussed here. Important aspects are the identification of breaklines, and a right degree of smoothing to eliminate height variations caused by noise while preserving real height variation patterns.

Fig. 10 illustrates this last step of DEM production. It shows the results of a test carried out in Milan in summer 1991 with a 1000 x 1000 subimage of one of the stereopairs of the OEEPE test data. A set of 2350 conjugate image points were measured with a mouse on the screen of a Microvax 3200 workstation. Successively, their 3-D ground coordinates were determined by space resection, using the results of a triangulation adjustment. The continuous surface, which was fitted to the set of points was a bicubic spline on a 300 m grid. Bicubic splines are patches of bicubic polynomials, which fit smoothly end to end at the borders of the patches. As no ground truth was available, no quantitative precision estimate could be made of the derived DEM. However, comparing the bicubic spline surface with that obtained by simply triangulating the determined points nicely shows how the imposition of smoothness conditions improves the precision of the single heights there where points are dense with respect to terrain variations. It also shows how improbable terrain features are 'invented' in areas where points are too sparse. Some of the too sparsely sampled areas correspond to forests, which produce homogeneous image areas (i.e. without grey level gradients).

5 CONCLUSIONS

An analysis has been made of the factors determining the precision of a DEM derived from stereo SPOT data. The first factor is the determination of the precise imaging geometry in a triangulation adjustment. By careful modelling, a sufficiently precise description of the imaging geometry can be obtained with only a limited number of ground control points. This is remarkable considering the many parameters, which are involved. Average conjugate image points can be measured with a r.m.s.e of 0.5 pixel for both row and column coordinate. Considering only the geometry of the intersecting imaging rays, this corresponds, for a 21° E / 21° W stereo pair, at ground level to a positioning precision of about 4m, 4m and 8m for the along-track, across-track and height coordinate respectively. To this, the uncertainty in the knowledge of the imaging geometry must be added. The imposition of smoothness conditions by the fitting of a continuous surface to the estimated ground points can improve height precision in areas where points are dense with respect to terrain variations.

6 ACKNOWLEDGEMENTS

This paper is based on experiences obtained during the author's participation to the OEEPE test on triangulation with SPOT data and successive research. The author wishes to express his gratitude to the OEEPE and IGN for their contributions to the OEEPE project. Partial funding of the research by the Commission of the European Communities and OMI-Agusta Spa is gratefully acknowledged.

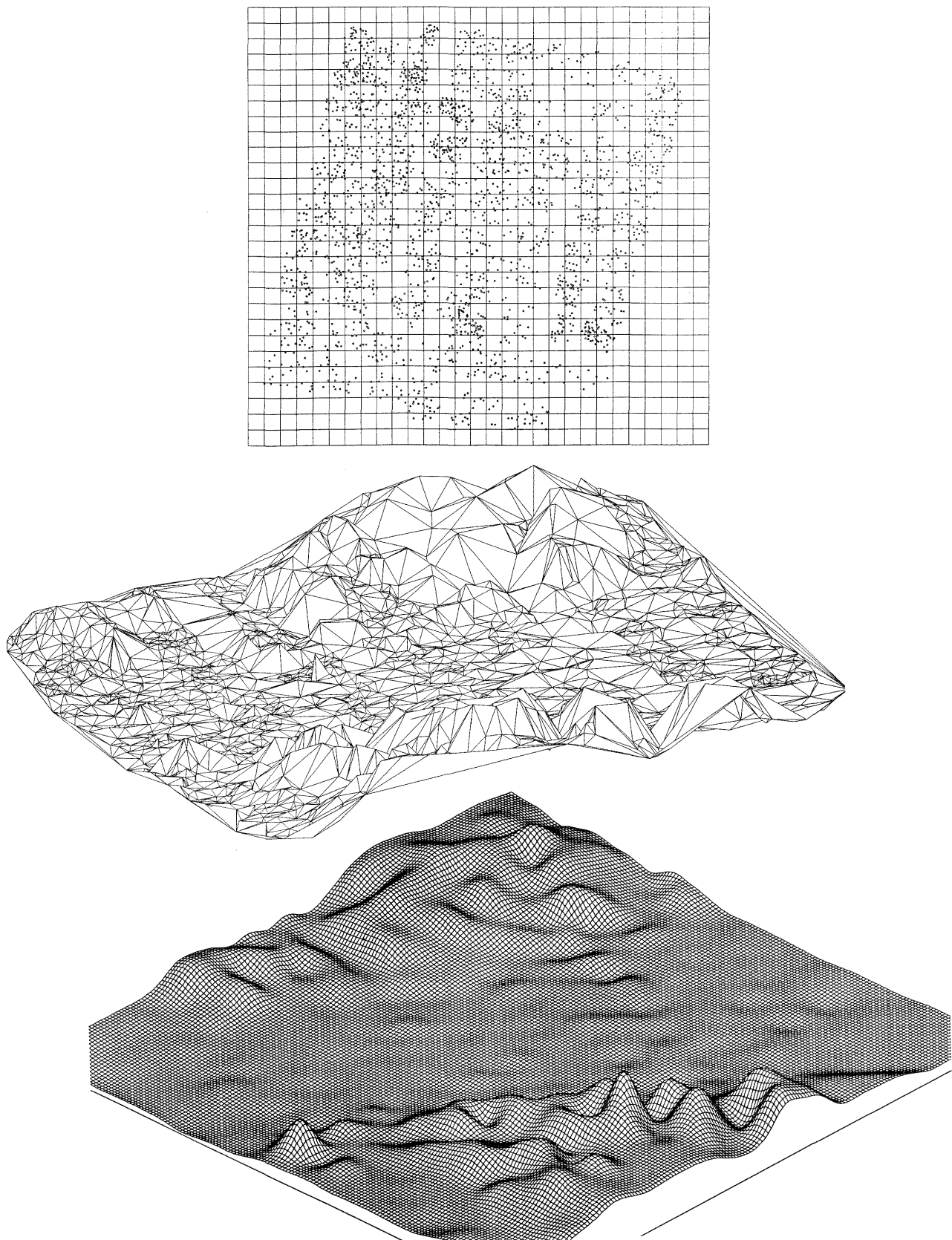


Fig. 10 -

Planimetric distribution of determined ground points and the grid for bicubic spline interpolation;

Surface obtained by simple triangulation of the determined points (no smoothness condition imposed);

Smooth surface obtained by the fitting of a bicubic spline.

REFERENCES

- Brockelbank, D.C., Cam, A.P., (1991). Stereo elevation determination techniques for SPOT imagery. *Photogrammetric Engineering and Remote Sensing*, 57 (8): 1065-1073.
- Chen, L.C., Lee, L.H., Lee, S.C., (1988). DTM generation using SPOT digital data. In: *Int. Arch. Photogramm. Remote Sensing, Kyoto-Japan, Vol. 27, Part B3*, pp. 100-109.
- Chevrel, M., Courtois, M., Weill, G., (1981). The SPOT satellite remote sensing mission. *Photogrammetric Engineering and Remote Sensing*, 47 (8): 1163-1171.
- Day, T., Muller, J.-P., (1988). Quality assesment of digital elevation models produced by automatic stereo matchers from SPOT image pairs. In: *Int. Arch. Photogramm. Remote Sensing, Kyoto-Japan, Vol. 27, Part B3*, pp. 148-159.
- Dowman, I.J., Neto, F., (1992). Triangulation with SPOT data at University College London. In: Dowman, I.J., (Ed.) (1992). *OEEPE test of triangulation of SPOT data, OEEPE*.
- Friedmann, D., Friedel, J., Magnussen, K., Kwok, R., Richardson, S., (1983). Multiple scene precision rectification of spaceborn imagery with very few control points. *Photogrammetric Engineering and Remote Sensing*, 49 (12): 1657-1667.
- Grün, A., 1982. The accuracy potential of the modern bundle block adjustment in aerial photogrammetry. *Photogrammetric Engineering and Remote Sensing*, 48 (1): 45-54.
- Gülch, E., 1991. Results of test on image matching of ISPRS WG III/4. *ISPRS Journal of Photogrammetry and Remote Sensing*, 46 (2): 1-18.
- de Haan, A., (1991). A mathematical model for bundle adjustments with SPOT data. *Bollettino di Geodesia e Scienze Affini*, 50 (4): 253-272.
- de Haan, A., (1992). Contribution to the Politecnico di Milano to the OEEPE test on triangulation with SPOT data. In: Dowman, I.J., (Ed.) (1992). *OEEPE test of triangulation of SPOT data, OEEPE*.
- Heipke, C., Kornus, W., (1991). Nonsemantic photogrammetric processing of digital imagery - the example of SPOT stereo scenes. In: Ebner, H., Fritsch, D., Heipke, C., (Eds) (1991). *Digital Photogrammetric Systems*, pp. 86-102, Wichmann, Karlsruhe.
- Konecny, G., (1988). Geometric evaluation of SPOT imagery. CERCO seminar on the SPOT system and its applications, Paris, June 6-9, 1988.
- Kratky, V. (1992). Rigorous photogrammetric processing of SPOT images at CCM, Canada. In: Dowman, I.J., (Ed.) (1992). *OEEPE test of triangulation of SPOT data, OEEPE*.
- Kubik, K., (1970). The estimation of weights of the measured quantities within the method of least squares. *Bulletin Géodésique*, (95): 21-40.
- Murray, K., Newby, P., (1988). Mapping from SPOT imagery at the Ordnance Survey. In: *Int. Arch. Photogramm. Remote Sensing, Tsukuba-Japan, Vol. 28, Part 4*, pp. 430-438.
- Picht, G., Kruck, E., Guretzki, M., (1992). Processing of SPOT image blocks with program BINGO. In: Dowman, I.J., (Ed.) (1992). *OEEPE test of triangulation of SPOT data, OEEPE*.
- Priebbenow, R., (1992). Triangulation of SPOT imagery at the Department of Lands, Queensland. In: Dowman, I.J., (Ed.) (1992). *OEEPE test of triangulation of SPOT data, OEEPE*.
- Rosenholm, D., 1987. Empirical investigation of optimal window size using the least squares image matching method. *Photogrammetria*, 42 (3): 113-125.
- Sansò F., Rummel R. (Eds.) 1989. *Theory of satellite geodesy and gravity field determination*. Springer-Verlag, Berlin.
- Sharpe, B., Wiebe K., 1988. Reduction of ground control requirements by pass processing. In: *Int. Arch. Photogramm. Remote Sensing, Kyoto-Japan, Vol. 27, Part B4*, pp. 350-357.
- Spotimage, 1988. *SPOT User handbook*. CNES and Spotimage, Toulouse.
- Theodossiou, E.I., Dowman I.J., (1990). Heighting accuracy of SPOT. *Photogrammetric Engineering and Remote Sensing*, 56 (12): 1643-1649.
- Veillet, I., (1992). Triangulation of SPOT data for the OEEPE test at IGN. In: Dowman, I.J., (Ed.) (1992). *OEEPE test of triangulation of SPOT data, OEEPE*.
- Westin, T., (1991). Precision rectification of SPOT imagery. In: *Photogrammetric Reports No. 55*, Royal Institute of Technology, Department of Photogrammetry, Stockholm, Sweden.